Smart Materials and Structures

PURPOSE-LED PUBLISHING™

PAPER

IPMC mechanoelectrical transduction: its scalability and optimization

To cite this article: D Pugal *et al* 2013 *Smart Mater. Struct.* **22** 125029

View the article online for updates and enhancements.

You may also like

- Characterizing the transduction behavior of ionic polymer-metal composite actuators and sensors via dimensional analysis
Zakai J Olsen and Kwang J Kim
- Mechanoelectrical impedance of a carbide-derived carbon-based laminate motion sensor at large bending deflections
Indrek Must, Mart Anton, Erki Viidalepp et al.
- A hyperelastic porous media framework for ionic polymer-metal composite actuators and sensors: thermodynamically consistent formulation and nondimensionalization of the field equations
Zakai J Olsen and Kwang J Kim

This content was downloaded from IP address 131.216.14.8 on 07/04/2026 at 18:51

Smart Mater. Struct. **22** (2013) 125029 (8pp) doi:10.1088/0964-1726/22/12/125029

IPMC mechanoelectrical transduction: its scalability and optimization

D Pugal[1,2], P Solin[3,4], A Aabloo[2] and K J Kim[5]

[1] Mechanical Engineering Department, University of Nevada, Reno, NV, USA
[2] Institute of Technology, Tartu University, Estonia
[3] Department of Mathematics and Statistics, University of Nevada, Reno, NV, USA
[4] Institute of Thermomechanics, Prague, Czech Republic
[5] Department of Mechanical Engineering, University of Nevada, Las Vegas, NV, USA

E-mail: david.pugal@gmail.com and kwang.kim@unlv.edu

Received 8 August 2013
Published 22 November 2013
Online at stacks.iop.org/SMS/22/125029

Abstract
Ionic polymer–metal composite (IPMC) mechanoelectrical transduction is described with a system of partial differential equations—the Poisson equation, the Nernst–Planck equation, and the Navier equations for the displacements. Modeling of this system of four equations is challenging due to the differences in the physical fields—namely, one physical field can be very smooth while others have steeper gradients. When using the conventional finite element method (FEM), the problem size in terms of number of degrees of freedom can be very large. Additionally, it is challenging to find an optimal mesh due to the fact that the physical fields are time dependent. Last but not least, due to the coupled nature of the system, it is necessary to have a way to estimate the error to ensure the desired accuracy of the solutions. In this work, we propose a novel *hp*-FEM modeling method for solving the system of equations. *hp*-FEM is a modern version of the FEM that is capable of exponential convergence. It is also demonstrated how the multi-meshing reduces the problem size while maintaining the prescribed error limit. The solution domain that describes IPMC can be scaled without a significant increase in the number of degrees of freedom and solution time. Additionally, PID controller based time step optimization is incorporated. The model is implemented in Hermes, which is a free *hp*-FEM solver.

(Some figures may appear in colour only in the online journal)

1. Introduction

Ionic polymer–metal composite (IPMC) consists of a thin ionomeric polymer membrane. A commonly used material is Nafion [1, 2]. Typically, the membrane is electrolessly coated with an electrode such as platinum. The polymer membrane contains fixed anions and solvent with freely movable cations, so the overall charge of the material is balanced.

IPMCs have been widely studied for their potential to serve as noiseless electromechanical transducers [3–11]. The advantages of IPMC over other electroactive polymer actuators are low voltage bending, high strains (over 1%), and the ability to work in wet environments.

While plenty of research on IPMC electromechanical transduction has been carried out, the number of papers considering the mechanoelectrical transduction or voltage/current sensory properties of IPMC is much smaller. Regardless, a number of applications such as devices for blood pressure and pulse measurement [12], pressure transducers in the human spine [13], and vibration sensing transducers [14] have been proposed.

At the same time, there are various ways in which the physics behind the mechanoelectrical transduction of IPMCs is understood. Tadokoro *et al* proposed a model of ionic polymers based on the ionic motion [15]. Other authors explained the underlying causes of the transduction with solvent fluxes and pressure gradients based on the standard Onsager relations [16–18]. In such systems, the induced electric field is proportional to the applied bending torque, which causes a pressure gradient in the material. A different

 © 2013 IOP Publishing Ltd Printed in the UK & the USA

approach to describe the mechanoelectrical transduction is to consider the electrostatic interaction within the polymer. The model was first proposed by Nemat-Nasser and Li [19, 1]. While the charge sensing in this model is connected to ionic dipoles that are induced in the polymer clusters, Farinholt and Leo, based on the same field equations, presented a hypothesis that the charge density on the surface of the polymer is proportional to the induced stress [20]. Chen *et al* used the same underlying equations as Farinholt and Leo, but expanded the model and added the effects of electrode resistance [21]. This resulted in a compact, transfer-function representation of the physics based model.

1.1. Motivation

Our ongoing research on the mechanoelectrical transduction of IPMC materials has been focused on thorough understanding of the underlying physics. More precisely, from the fundamental aspect, we have developed a physics based model that is based on the boundary conditions that can be easily measured and applied to reduce the number of unknown parameters. From the engineering aspect, we have been actively researching various methods to model the equations efficiently. This paper focuses mainly on the engineering aspect. After introducing the model of mechanoelectrical transduction, we demonstrate in detail how the novel *hp*-FEM method can be applied in modeling the phenomenon. IPMC material is modeled via a multi-physics coupled problem consisting of the Poisson and Nernst–Planck equations (further abbreviated by PNP) and the Navier equations for the displacement. These equations are used to calculate the charge transport and resulting electromechanical transduction using the *hp*-FEM (finite element method). The computing power required for a full scale problem of the PNP coupled to the Navier equations can be significant. Furthermore, the calculated field shape and magnitudes depend on the chosen material constants and also the material thickness—for instance, the distance between the electrodes significantly affects the transported charge near the electrodes and thus also both the potential and cation concentration gradients. This makes the choice of an optimal mesh for FEM calculations problematic and is the reason why we are interested in exploring adaptive algorithms—it is demonstrated how using the novel *hp*-FEM helps to keep the problem size small in terms of the number of degrees of freedom (*n*DOF) while automatically maintaining a pre-set maximum error of the solution. Moreover, *hp*-FEM helps to keep the problem geometrically scalable—there is no need to manually change a mesh after changing problem parameters such as the calculation domain dimensions. Additionally, it is shown how employing a PID controller based time step adaptivity helps to reduce the calculation time. The demonstrated method is based on a study that was first presented at the SPIE conference in San Diego [22].

2. IPMC mechanoelectrical transduction model

The underlying cause of the phenomenon of electromechanical and mechanoelectrical transduction is induced ionic current and resulting non-zero spatial charge in the vicinity of the electrodes. The ionic current in the polymer is calculated with the Nernst–Planck equation,

$$\frac{\partial C}{\partial t} + \nabla \cdot (-D\nabla C - z\mu FC\nabla\phi - \mu C\Delta V\nabla P) = 0, \quad (1)$$

where C is the cation concentration, μ is the mobility of the cations, D is the diffusion constant, F is the Faraday constant, z is the charge number, ΔV is the molar volume which quantifies the cation hydrophilicity, P is the solvent pressure, and ϕ is the electric potential in the polymer. The Poisson equation governs the electric potential and has the form

$$-\nabla^2\phi = \frac{F\rho}{\varepsilon} \quad (2)$$

where ε is the absolute dielectric permittivity. The charge density $\rho = C - C_a$ where C_a is the local anion concentration.

Equation (1) is the main governing equation for describing the transduction phenomena of the IPMC materials. Besides the time derivative term, the equation consists of three flux terms governed by different field gradients, namely, the electric potential gradient $\nabla\phi$, the concentration gradient ∇C, and the solvent pressure gradient ∇P. These field gradients exist for both transduction types, albeit with significantly different magnitudes.

Conceptual models of IPMC electromechanical and mechanoelectrical transduction with the field gradients are shown in figures 1 and 2, respectively. The potential gradient $\nabla\phi$ has the opposite direction in the case of mechanoelectrical transduction, because the ionic current is not governed by an applied voltage but by a bending induced pressure gradient ∇P.

The linear elastic material model is used to describe the deformation of IPMC. In 2D Cartesian coordinates the Navier

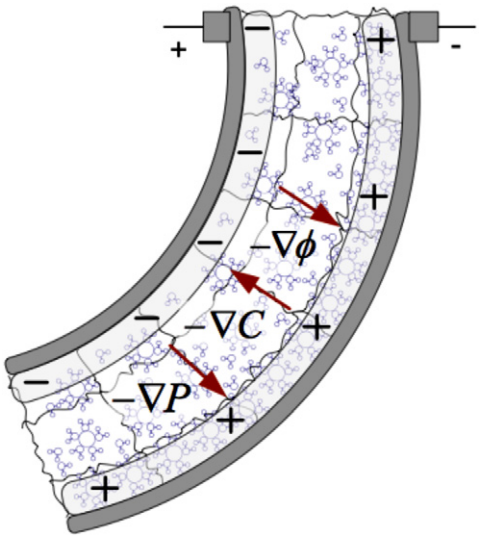

Figure 1. IPMC electromechanical transduction model with the formed field gradients.

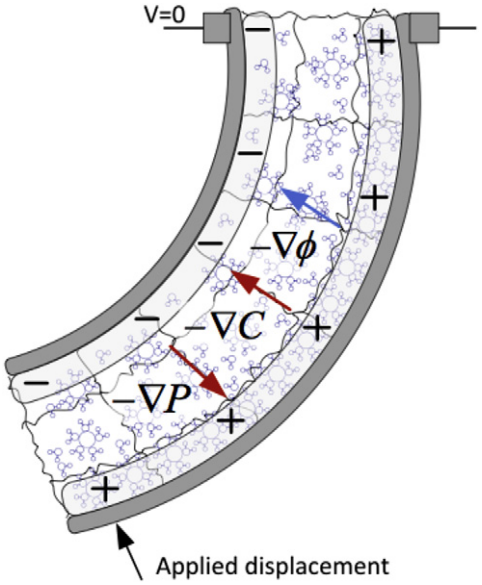

Figure 2. IPMC mechanoelectrical transduction model with the formed field gradients.

equations take the form

$$(\lambda+\mu)\left(\frac{\partial^2 u_1}{\partial x^2}+\frac{\partial^2 u_2}{\partial y \partial x}\right)+\mu\left(\frac{\partial^2 u_1}{\partial x^2}+\frac{\partial^2 u_1}{\partial y^2}\right)+F_1=0, \tag{3}$$

$$(\lambda+\mu)\left(\frac{\partial^2 u_1}{\partial x \partial y}+\frac{\partial^2 u_2}{\partial y^2}\right)+\mu\left(\frac{\partial^2 u_2}{\partial x^2}+\frac{\partial^2 u_2}{\partial y^2}\right)+F_2=0. \tag{4}$$

In the case of IPMC electromechanical transduction, $F_2 = 0$ and F_1 can be expressed as a function of cation concentration, $F_1 = A(C - C_a)$, where A is a constant [23]. For mechanoelectrical transduction, the body force can be neglected and the bending is governed by appropriate boundary conditions. The constants λ and μ are Lame's constants

$$\mu=\frac{E}{2(1+\nu)}, \qquad \lambda=\frac{\nu E}{(1+\nu)(1-2\nu)} \tag{5}$$

where E is Young's modulus and ν is Poisson's ratio.

Our research shows that although the provided equations describe both transduction types of IPMC, some terms are more prevalent than others for different transductions. For instance, it is reasonable to neglect the third flux term in (1) in the case of electromechanical transduction as it is very small compared to the second term. Also, while the local cation concentration can be expressed as a constant in the case of electromechanical transduction, it plays an important role in mechanoelectrical transduction where the field gradients are significantly smaller.

In the following, coupling of the Navier equations and the Nernst–Planck equation is demonstrated based on a simplified model where $C_a = C_0$ is a constant and $\Delta V \nabla P \approx 0$.

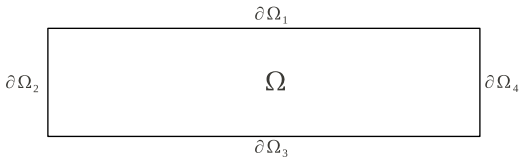

Figure 3. The calculation domain $\Omega \subset \mathbb{R}^2$ with boundaries $\partial\Omega_{1\ldots4} \subset \partial\Omega$.

3. Modeling approach

IPMC material is modeled via a multi-physics coupled problem, consisting of the PNP system of equations coupled to the Navier equations. A rectangular 2D domain $\Omega \subset \mathbb{R}^2$ with boundaries $\partial\Omega_{1\ldots4} \subset \partial\Omega$ as shown in figure 3 is considered. The height of the domain (boundaries $\partial\Omega_1$ and $\partial\Omega_3$) is varied from 0.2 to 1 mm whereas the length is fixed to 1 mm in the calculations.

The simplified form of the Nernst–Planck equation (1) for the mobile cations has the form

$$\frac{\partial C}{\partial t}+\nabla\cdot(-D\nabla C-\mu F C\nabla\phi)=0. \tag{6}$$

As there is no flow through the domain's boundary, equation (6) is equipped with a Neumann boundary condition (BC)

$$-D\frac{\partial C}{\partial n}-\mu F C\frac{\partial \phi}{\partial n}=0. \tag{7}$$

A positive constant voltage V_{pos} BC is prescribed on $\partial\Omega_1$ and a zero voltage BC on $\partial\Omega_3$,

$$\phi_{\partial\Omega_1}=V_{pos}, \qquad \phi_{\partial\Omega_3}=0. \tag{8}$$

On the rest of the boundary, ϕ has zero normal derivatives, and it is thus equipped with Neumann BCs

$$\frac{\partial \phi_{\Omega_2}}{\partial n}=\frac{\partial \phi_{\Omega_4}}{\partial n}=0. \tag{9}$$

For the Navier equations (3) and (4), the following Dirichlet BCs are applied:

$$u_{1_{\partial\Omega_2}}=u_{2_{\partial\Omega_2}}=0. \tag{10}$$

As no external forces are considered, zero Neumann BCs are applied on $\partial\Omega$ for the Navier equations. To make the results easily reproducible, in the following the weak form of equations (6), (2), (3), (4) is presented—the Jacobian and the residual vector can be effortlessly derived from the weak form for finite element calculations.

3.1. Dimensionless weak form of the equations

To simplify the notation, a dimensionless formulation of the equations is used. The following new notations for the independent variables x, y, t and for the dependent variables

cation concentration C and electric potential ϕ are used [24]:

$$X = \frac{x}{l}, \qquad Y = \frac{y}{l},$$
$$\tau = \frac{tD}{\lambda_D l}, \qquad \varphi = \frac{\phi F}{RT}, \tag{11}$$
$$c = \frac{C}{C_0}, \qquad U_1 = \frac{u_1}{l}, \qquad U_2 = \frac{u_2}{l}.$$

Here λ_D is the Debye screening length and ϵ is its dimensionless form and they are expressed as follows:

$$\lambda_D = \sqrt{\frac{\varepsilon RT}{2F^2 C_0}}, \qquad \epsilon = \frac{\lambda_D}{l}. \tag{12}$$

For the dimensionless gradient, the following notation is used:

$$\nabla_d = \left(\frac{\partial}{\partial X}, \frac{\partial}{\partial Y}\right). \tag{13}$$

Thus, the dimensionless form of the PNP system of equations is

$$\frac{\partial c}{\partial \tau} - \epsilon \nabla_d^2 c - \epsilon \nabla_d \cdot (c \nabla_d \varphi) = 0 \tag{14}$$

$$-\nabla_d^2 \varphi = \frac{c-1}{2\epsilon^2}. \tag{15}$$

The boundary condition (7) has the form

$$-\frac{\partial c}{\partial n} - c\frac{\partial \varphi}{\partial n} = 0. \tag{16}$$

The weak form of the Nernst–Planck equation is [25]

$$\int_\Omega \frac{\partial c}{\partial \tau} v^c \mathrm{d}\mathbf{x} + \epsilon \int_\Omega \nabla_d c \cdot \nabla_d v^c \mathrm{d}\mathbf{x} + \epsilon \int_\Omega c(\nabla_d \varphi \cdot \nabla_d v^c)\mathrm{d}\mathbf{x} = 0 \tag{17}$$

and the weak form of the Poisson equation is

$$\int_\Omega \nabla_d \varphi \cdot \nabla_d v^\varphi \mathrm{d}\mathbf{x} - \frac{1}{2\epsilon^2}\left[\int_\Omega c v^\varphi \mathrm{d}\mathbf{x} - \int_\Omega v^\varphi \mathrm{d}\mathbf{x}\right] = 0. \tag{18}$$

The dimensionless weak formulation of the Navier equation (3) is

$$\left(1 + \frac{\nu}{1-2\nu}\right)\int_\Omega \frac{\partial U_1}{\partial X}\frac{\partial v^{U_1}}{\partial X}\mathrm{d}\mathbf{x} + \frac{\nu}{1-2\nu}\int_\Omega \frac{\partial U_2}{\partial Y}\frac{\partial v^{U_1}}{\partial X}\mathrm{d}\mathbf{x} + \frac{1}{2}\int_\Omega \frac{\partial U_1}{\partial Y}\frac{\partial v^{U_1}}{\partial Y} + \frac{\partial U_2}{\partial X}\frac{\partial v^{U_1}}{\partial Y}\mathrm{d}\mathbf{x} + \frac{1+\nu}{E} C_0 l A \int_\Omega (1-c) v^{U_1}\mathrm{d}\mathbf{x} = 0. \tag{19}$$

Notice that the LHS consists only of dimensionless constants and variables and the displacements are governed solely by the RHS term which consists of material properties and is also a function of the cation concentration c,

$$f(c) = \frac{1+\nu}{E} C_0 l A \int_\Omega (c-1) v^{U_1}\mathrm{d}\mathbf{x}.$$

The function $f(c)$ can be considered as the governing term of IPCM electromechanical transduction in the weak formulation of the problem. Similarly, the dimensionless weak form of the Navier equation (4) is

$$\left(1 + \frac{\nu}{1-2\nu}\right)\int_\Omega \frac{\partial U_2}{\partial Y}\frac{\partial v^{U_2}}{\partial Y}\mathrm{d}\mathbf{x} + \frac{\nu}{1-2\nu}\int_\Omega \frac{\partial U_1}{\partial X}\frac{\partial v^{U_2}}{\partial Y}\mathrm{d}\mathbf{x} + \frac{1}{2}\int_\Omega \frac{\partial U_2}{\partial X}\frac{\partial v^{U_2}}{\partial X} + \frac{\partial U_1}{\partial Y}\frac{\partial v^{U_2}}{\partial X}\mathrm{d}\mathbf{x} = 0. \tag{20}$$

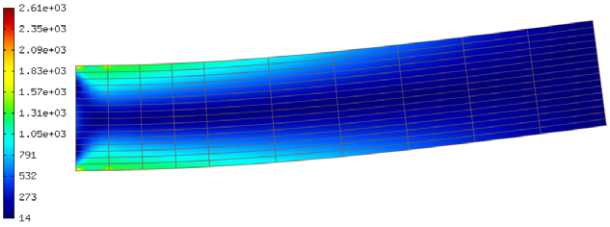

Figure 4. Example deformation of IPMC calculated with the Hermes *hp*-FEM software package. The color indicates local von-Mises stress.

4. *hp*-FEM implementation, scalability, and optimization

The *hp*-FEM is a modern version of the finite element method (FEM) that is capable of exponential convergence (the approximation error drops exponentially as new degrees of freedom are added during adaptivity) while standard FEM can only attain algebraic (polynomial) convergence rates which are much slower [26]. Hermes[6] is a free and open-source C++ library that implements higher-order finite elements approximations and adaptive *hp*-FEM. It supports eight different adaptivity modes—three isotropic and five anisotropic. It has been shown that for the given problem, the isotropic adaptivities are rather inefficient [25]. The supported anisotropic refinement modes are *h*-anisotropic (H_ANISO), *hp*-anisotropic-*h* (HP_ANISO_H), *p*-anisotropic (P_ANISO), *hp*-anisotropic-*p* (HP_ANISO_P), and *hp*-anisotropic (HP_ANISO). It must be noted that in the case of HP_ANISO_H, only the element size is adapted anisotropically whereas the polynomial degree is adapted isotropically. The opposite holds true for HP_ANISO_P.

In multi-physics PDE systems such as PNP, one physical field can be very smooth while others are not. If all the fields are approximated on the same mesh, then unnecessary refinements will be present in smooth areas where they are not necessary. This can be very wasteful. Hermes implements a novel adaptive multi-mesh *hp*-FEM [27–29] that makes it possible to approximate different fields on individual meshes.

The PNP–Navier problem was implemented in Hermes and a large number of calculations were carried out in order to find the best adaptivity mode. Furthermore, multi-mesh and single-mesh calculations were compared for CPU time and problem size in terms of number of degrees of freedom (*n*DOF). A deformation of IPMC calculated with Hermes is illustrated in figure 4.

[6] http://hpfem.org/hermes.

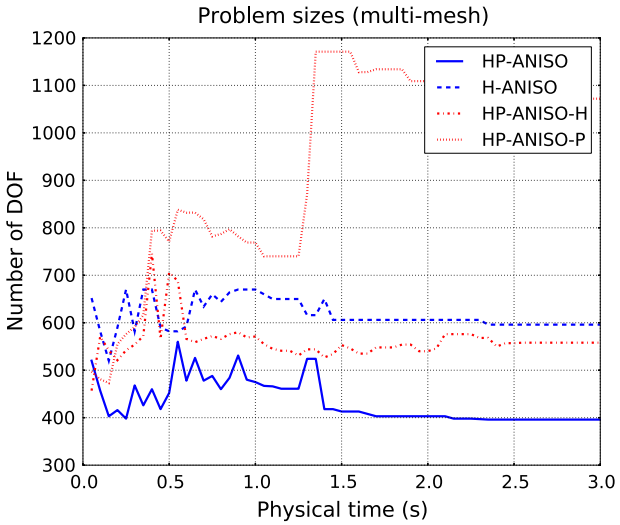

Figure 5. Problem size with different adaptivity modes in the multi-mesh configuration.

Figure 6. Problem time with different adaptivity modes in the multi-mesh configuration.

A number of comparative calculations showed that multi-mesh results in the smallest problem size with relatively small penalty to the computation time (or CPU time). Thus, the multi-mesh configuration was used for all simulations while the maximum relative error of a solution was fixed to 1.0%.

4.1. Advantages of anisotropic hp-adaptivity

The calculations were carried out with four different anisotropic adaptivity modes—H_ANISO, HP_ANISO, HP_ANISO_H, and HP_ANISO_P. It has already been shown that the rest of the adaptivity types (all isotropic, P_ANISO) do not perform well for this type of multi-physics problem [25]. For instance, in case of the *p*-adaptivities, it is necessary to know the problem and gradients rather well to start with a suitable initial mesh or the error might never converge below the pre-set limit; however, this would defeat the purpose of the automatic adaptivity. Therefore, comparative calculations of the PNP–Navier problem with H_ANISO, HP_ANISO, HP_ANISO_H, and HP_ANISO_P adaptivity modes were carried out and both problem size (*n*DOFs) and CPU time were recorded. Results for a 0.2 mm × 1 mm IPMC subjected to 1 V are shown in figures 5 and 6. It can be clearly seen that HP_ANISO adaptivity results in the best performance compared to the other anisotropic adaptivity types. Based on these results and also a number of other calculations that can be found in [25] (PNP system only), HP_ANISO adaptivity was chosen for the rest of the calculations in this work.

4.2. Geometry effects

Although the typical length of an IPMC is in the range of 1 cm and above, the calculations were carried out for 1 mm long IPMC. It turns out that increasing the length of the calculation domain will not result in significant penalty either in problem size or in CPU time. For the most part, the gradients in the longitudinal direction are small—even in the case where a potential drop along the boundaries $\partial\Omega_1$ and $\partial\Omega_3$ is considered.

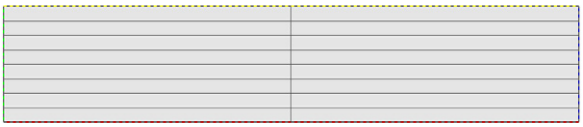

Figure 7. 0.2 mm thick IPMC initial mesh.

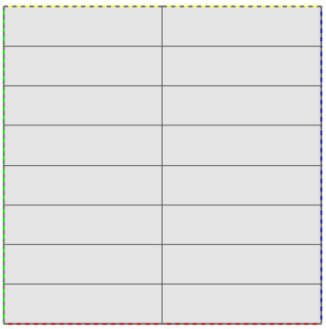

Figure 8. 1.0 mm thick IPMC initial mesh.

On the other hand, very steep gradients form in the thickness direction of IPMC. To study how *hp*-FEM performs for different IPMC dimensions, calculations were carried out for 0.2, 0.5, and 1.0 mm thick IPMCs. The initial mesh was the same for each thickness (see figures 7 and 8).

Figure 9 shows that the problem size depends on the domain thickness only slightly. This can be expected as the major field gradients ($\nabla_d c$ and $\nabla_d \varphi$) still form near the electrode boundaries. However, the CPU time does increase noticeably with the thickness—see figure 10. To investigate the reasons behind this, the number of adaptivity steps it takes to reach the desired error level (figure 11 subplot) was recorded at each time step (figure 11 main plot). Interestingly, it takes almost twice as many steps to reach to the pre-set 1.0% error for 1.0 mm IPMC compared to 0.2 mm IPMC.

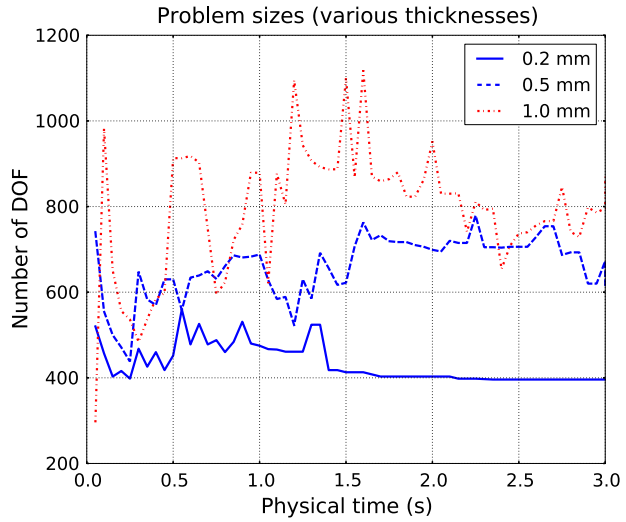

Figure 9. Problem size with final relative error at each time step for 0.2, 0.5, and 1.0 mm thick calculation domains.

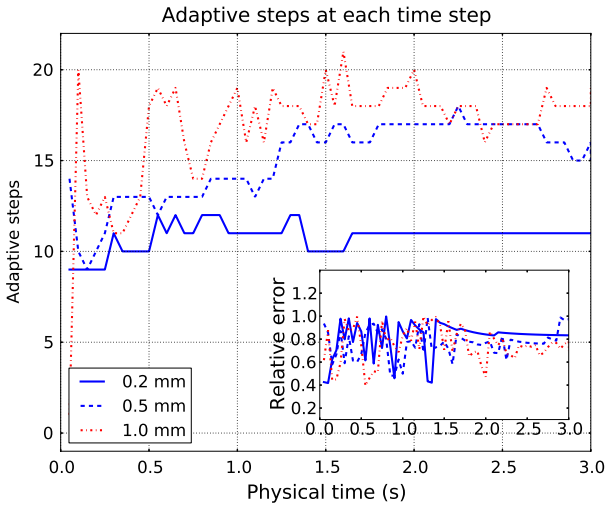

Figure 11. Number of adaptivity steps with final relative error at each time step for 0.2, 0.5, and 1.0 mm thick calculation domains.

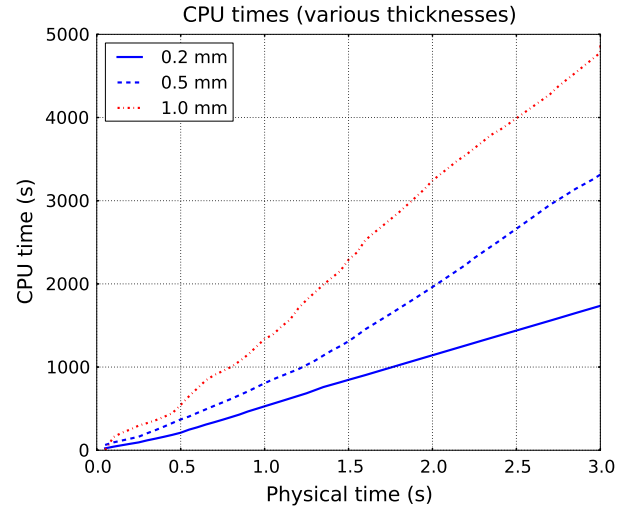

Figure 10. CPU time with final relative error at each time step for 0.2, 0.5, and 1.0 mm thick calculation domains.

Automatically refined meshes, field magnitudes, and polynomial spaces were captured for 0.2 and 1.0 mm thick IPMCs at $t = 0.1$ s to understand why the thicker IPMCs require so many extra adaptivity steps (figures 12 and 13). It can be seen that the displacement field calculation for 1.0 mm IPMC requires a considerably finer mesh and higher polynomial degrees near $\partial\Omega_2$—the effect of the fixed boundary is far more significant for a thick IPMC than for a 0.2 mm one with the same length. Refinements of the y-directional displacement field occur near the corners and inside the domain for the 1.0 mm IPMC and some elements have a polynomial degree of 7. At the same time, the potential field φ has a maximum polynomial degree of 4 and the meshes have been refined only near the boundaries $\partial\Omega_1$ and $\partial\Omega_3$ for both thicknesses, but the refinements are more significant near $\partial\Omega_1$ for 1.0 mm IPMC.

This example demonstrates how the *hp*-FEM adaptive algorithm can be beneficial in determining an optimal mesh and polynomial space for such a dynamic multi-physics problem. The use of a static mesh that is refined near the boundaries can work for some cases, but comparison of figures 12 and 13 shows how it might not be always sufficient to get precise calculation results while maintaining a small problem size.

4.3. Optimization

Although *hp*-FEM adaptive algorithms help to maintain a relatively small problem size in terms of *n*DOF during a time dependent calculation process, the CPU time can potentially be very high due to a large number of adaptivity steps. This is especially noticeable in the case of dynamic problems where the base mesh (see figures 7 and 8) is loaded at the beginning of each time step. To optimize the calculation time of HP_ANISO, an adaptive time step control was employed. The classical PID controller was used [25]. Since c, φ, U_1, and U_2 change differently in time, the relative changes between the solutions at different time steps were monitored,

$$e_c^n = \frac{\|c^n - c^{n-1}\|}{\|c^n\|}, \tag{21}$$

$$e_\varphi^n = \frac{\|\varphi^n - \varphi^{n-1}\|}{\|\varphi^n\|}, \tag{22}$$

$$e_{U_1}^n = \frac{\|U_1^n - U_1^{n-1}\|}{\|U_1^n\|}, \tag{23}$$

$$e_{U_2}^n = \frac{\|U_2^n - U_2^{n-1}\|}{\|U_2^n\|}. \tag{24}$$

The relative changes to control the time step were calculated as follows:

$$e^n = \max\{e_c^n,\ e_\varphi^n,\ e_{U_1}^n,\ e_{U_2}^n\}. \tag{25}$$

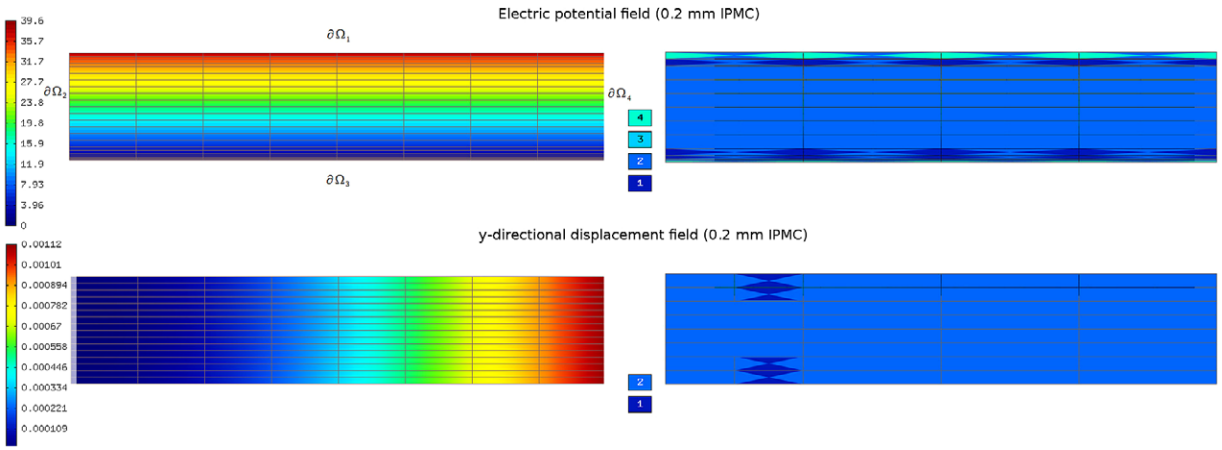

Figure 12. 0.2 mm thick IPMC calculation snapshot at $t = 0.1$ s. Mesh and magnitudes of φ and U_2 (left); polynomial degrees of φ and U_2 (right). The top left image also shows the domain boundaries as shown in figure 3.

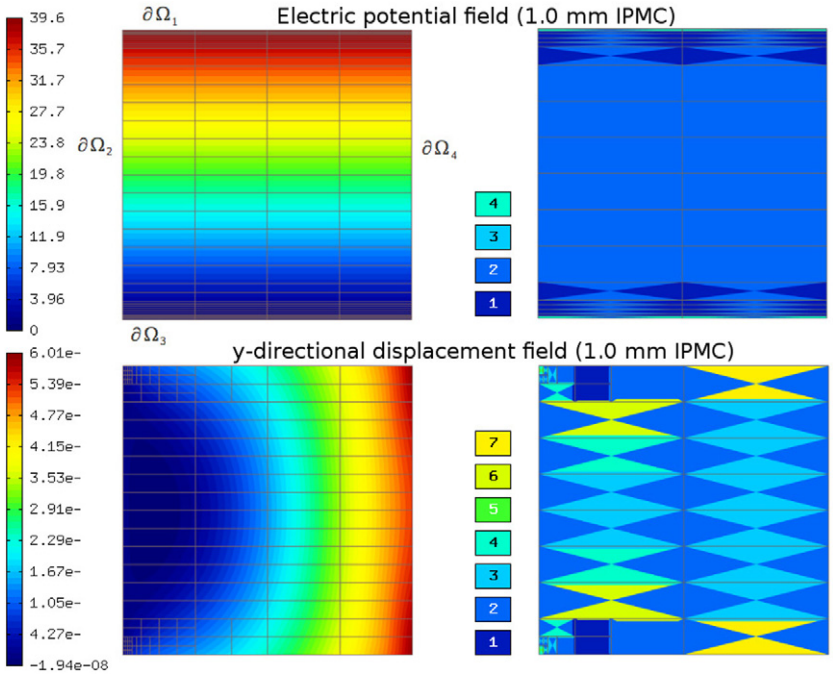

Figure 13. 1.0 mm thick IPMC calculation snapshot at $t = 0.1$ s. Mesh and magnitudes of φ and U_2 (left); polynomial degrees of φ and U_2 (right). The top left image also shows the domain boundaries as shown in figure 3.

If $e^n < \delta$, where $\delta > 0$ is a defined tolerance, then the time step for the next iteration is increased smoothly to

$$\delta\tau^{n+1} = \left(\frac{e^{n-1}}{e^n}\right)^{k_P} \left(\frac{\delta}{e^n}\right)^{k_I} \left[\frac{(e^{n-1})^2}{e^n e^{n-2}}\right]^{k_D} \delta\tau^n \quad (26)$$

where the parameters are [30]

$$k_p = 0.075, \qquad k_I = 0.175, \qquad k_D = 0.01. \quad (27)$$

The tolerance δ was set to $\delta = 0.25$ in the current optimization example. The HP_ANISO problem size and computing time with and without the time step control are shown in figures 14 and 15 for 0.2 and 1.0 mm IPMCs. It can be seen that the computing time was reduced more than two times when the time step control was employed. At the same time, the problem size was hardly affected at all.

5. Conclusions

In this work, an IPMC mechanoelectrical transduction model was proposed. The Nernst–Planck–Poisson–Euler system of equations based model was solved using the *hp*-finite element method with an adaptive multi-mesh configuration, implemented with the Hermes *hp*-FEM time dependent adaptive solver. It was demonstrated that by using the time dependent adaptivity, multi-mesh configuration, and anisotropic *hp* refinements, the problem size remains very small throughout the solving process while maintaining a

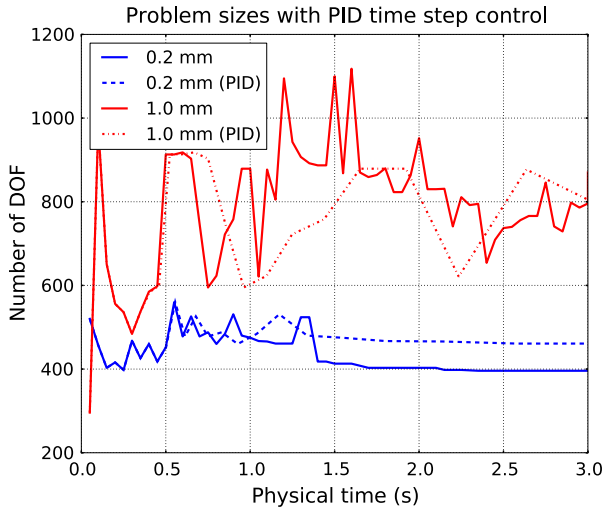

Figure 14. Problem sizes of 0.2 and 1.0 mm thick IPMCs with and without PID time step control.

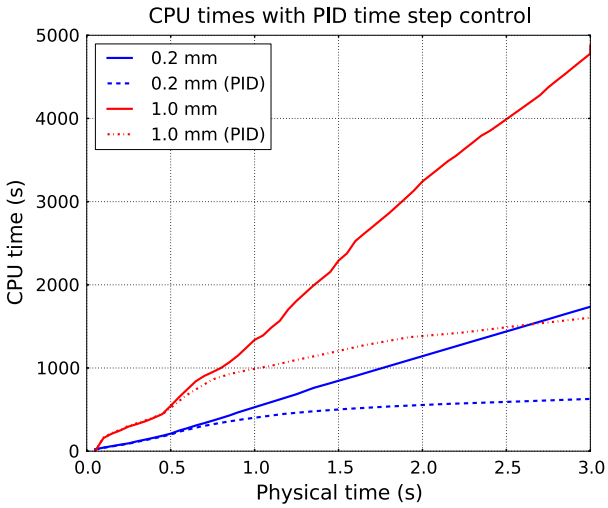

Figure 15. CPU times of 0.2 and 1.0 mm thick IPMCs with and without PID time step control.

pre-set relative error of the solution. Furthermore, due to *hp*-FEM automatic adaptivity, the problem is scalable for different geometry configurations. Various IPMC thicknesses were modeled and the problem size did not increase significantly with change of the thickness and aspect ratio of the calculation domain. However, the adaptivity can consume a lot of CPU time. It was shown that calculation times can be reduced more than a factor of two by employing a simple PID controller based time step adaptivity.

In conclusion, by using *hp*-FEM with an adaptive multi-mesh configuration, a small problem size of the Nernst–Planck–Poisson–Euler equation system can be achieved for different geometry configurations while still maintaining a prescribed precision of the solution.

Acknowledgments

KJK acknowledges partial financial support from the Office of Naval Research (N000141310274). AA and DP acknowledge ETF Grant ETF 8553. PS acknowledges Grant No. P102/11/0498 of the Grant Agency of the Czech Republic.

References

[1] Nemat-Nasser S 2002 *J. Appl. Phys.* **92** 2899–915
[2] Nemat-Nasser S and Wu Y 2003 *J. Appl. Phys.* **93** 5255–67
[3] Basu S and Sharma M 1997 *J. Membr. Sci.* **124** 77–91
[4] Shahinpoor M and Kim K J 2001 *Smart Mater. Struct.* **10** 819
[5] Newbury K and Leo D 2003 *J. Intell. Mater. Syst. Struct.* **14** 333
[6] Wallmersperger T, Leo D J and Kothera C S 2007 *J. Appl. Phys.* **101** 024912
[7] Porfiri M 2008 *J. Appl. Phys.* **104** 104915
[8] Pugal D, Kim K J, Punning A, Kasemagi H, Kruusmaa M and Aabloo A 2008 *J. Appl. Phys.* **103** 084908
[9] Pugal D, Jung K, Aabloo A and Kim K 2010 *Polym. Int.* **59** 279–89
[10] Rossiter J, Stoimenov B and Mukai T 2006 A bistable artificial muscle actuator *2006 Int. Symp. on Micro–NanoMechatronics and Human Science* pp 1–6
[11] Zangrilli U and Weiland L M 2011 *Smart Mater. Struct.* **20** 094013
[12] Keshavarzi A, Shahinpoor M, Kim K J and Lantz J W 1999 Blood pressure, pulse rate, and rhythm measurement using ionic polymer–metal composite sensors *Symp. on Smart Structures and Materials (Newport Beach, CA)* pp 369–76
[13] Ferrara L, Shahinpoor M, Kim K J, Schreyer B, Keshavarzi A, Benzel E and Lantz J 1999 *Smart Structures and Materials: Electroactive Polymer Actuators and Devices (Newport Beach, CA)* vol 3669, pp 394–401
[14] Paola B, Fortuna L, Giannone P, Graziani S and Strazzeri S 2008 Ipmcs as vibration sensors *IPMCS 2008: Instrumentation and Measurement Technology Conf. Proc., 2008* (Piscataway, NJ: IEEE) pp 2065–9
[15] Tadokoro S, Yamagami S, Takamori T and Oguro K 2000 Modeling of nafion-Pt composite actuators (ICPF) by ionic motion *Smart Materials and Structures: Electroactive Polymer Actuators and Devices* vol 3987, pp 92–102
[16] Asaka K and Oguro K 2000 *J. Electroanal. Chem.* **480** 186–98
[17] Gennes P G D, Okumura K, Shahinpoor M and Kim K J 2000 *Europhys. Lett.* **50** 513
[18] Shahinpoor M and Kim K 2002 *Appl. Phys. Lett.* **80** 3445–7
[19] Nemat-Nasser S and Li J Y 2000 *J. Appl. Phys.* **87** 3321–31
[20] Farinholt K and Leo D J 2004 *Mech. Mater.* **36** 421–33
[21] Chen Z, Tan X, Will A and Ziel C 2007 *Smart Mater. Struct.* **16** 1477
[22] Pugal D, Aabloo A and Kim K 2013 *Proc. SPIE* **8687** 86870X
[23] Pugal D, Kim K J and Aabloo A 2011 *J. Appl. Phys.* **110** 084904
[24] Bazant M, Thornton K and Ajdari A 2004 *Phys. Rev.* E **70** 21506
[25] Pugal D, Solin P, Kim K J and Aabloo A 2012 *Commun. Comput. Phys.* **11** 249–70
[26] Solin P, Segeth K and Dolezel I 2003 *Higher-Order Finite Element Methods* Chapman & Hall/CRC Press
[27] Solin P, Cerveny J, Dubcova L and Andrs D 2010 *J. Comput. Appl. Math.* **234** 2350–7
[28] Solin P, Dubcova L and Kruis J 2010 *J. Comput. Appl. Math.* **233** 3103–12
[29] Dubcova L, Solin P, Cerveny J and Kus P 2010 *Electromagnetics* **30** 23–40
[30] Valli A M P, Carey G F and Coutinho A 2002 *Commun. Numer. Methods Eng.* **18** 131–9